Mapping the Surface Adsorption Forces of Nanomaterials in Biological Systems

Xin R. Xia,[†] Nancy A. Monteiro-Riviere,[†] Sanjay Mathur,[‡] Xuefeng Song,[‡] Lisong Xiao,[‡] Steven J. Oldenberg,[§] Bengt Fadeel,[⊥] and Jim E. Riviere[†,*]

[†]Center for Chemical Toxicology Research and Pharmacokinetics, North Carolina State University, Raleigh, North Carolina 27607, United States, [‡]Institute of Inorganic Chemistry, University of Cologne, Cologne, Germany, [§]NanoComposix, San Diego, California 92111, United States, and [⊥]Institute of Environmental Medicine, Karolinska Institutet, SE-171 77 Stockholm, Sweden

ABSTRACT

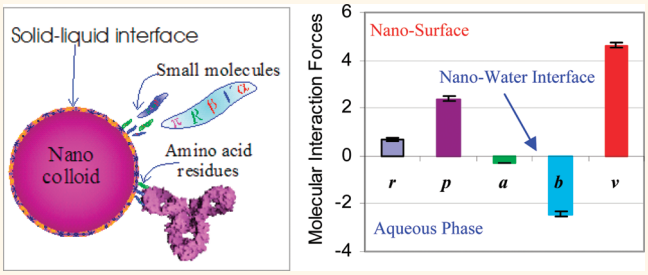

The biological surface adsorption index (BSAI) is a novel approach to characterize surface adsorption energy of nanomaterials that is the primary force behind nanoparticle aggregation, protein corona formation, and other complex interactions of nanomaterials within biological systems. Five quantitative nanodescriptors were obtained to represent the surface adsorption forces (hydrophobicity, hydrogen bond, polarity/polarizability, and lone-pair electrons) of the nanomaterial interaction with biological components. We have mapped the surface adsorption forces over 16 different nanomaterials. When the five-dimensional information of the nanodescriptors was reduced to two dimensions, the 16 nanomaterials were classified into distinct clusters according their surface adsorption properties. BSAI nanodescriptors are intrinsic properties of nanomaterials useful for quantitative structure—activity relationship (QSAR) model development. This is the first success in quantitative characterization of the surface adsorption forces of nanomaterials in biological conditions, which could open a quantitative avenue in predictive nanomedicine development, risk assessment, and safety evaluation of nanomaterials.

KEYWORDS: engineered nanomaterials · surface adsorption · risk assessment · nanotoxicology · nanomedicine · nanomaterial characterization

The complex interactions and dynamic changes of engineered nanomaterials in biological systems have hindered the rapid development of bionanoscience.[1−3] Colloidal nanoparticles are metastable suspensions that are subject to aggregation due to aging or changes in media conditions such as pH and ionic strength. The aggregation of engineered nanomaterials in media is one of the most problematic issues in biological studies of nanomaterials, which diminishes any meaning of careful characterization before *in vitro* or *in vivo* doses.[4,5] Another complication is the adsorption of biomolecules onto the surfaces of nanoparticles forming so-called nanoparticle—protein coronas that dynamically change in the biological milieu.[1,6−8] Further complication arises from nanoparticle—cell membrane interactions; once internalized, the nanoparticles are exposed to totally different biological environments.[9,10] These complicated interactions and dynamic changes of nanomaterials make a meaningful characterization of the nanoparticle surfaces properties in biological systems difficult.

Careful study of the mechanisms of the nanoparticle aggregation and protein corona formation processes suggests that the surface adsorption energy of the nanoparticles is the primary driving force behind all of these complicated interactions and dynamic changes of nanomaterials within biological systems. The surface adsorption energy is unique to the small size of nanoparticles with extremely high surface to volume ratio, where the unsaturated surface chemical bonds tend to adsorb other chemicals or biomolecules to reduce their surface energy.[1,11] A biological surface adsorption index (BSAI) was developed to characterize the surface adsorption energy of nanomaterials under biologically relevant aqueous conditions.[12]

The strategy of the BSAI approach is to measure the surface adsorption forces in idealized biological conditions, that is, a system that has the same medium conditions as *in situ* biological systems such as pH, ionic strength, and biomolecules that do not significantly interact with the surfaces of the nanomaterials. Under such idealized biological conditions, the surface adsorption properties can be measured using a set of probe compounds with diverse physicochemical

* Address correspondence to jim_riviere@ncsu.edu.

Received for review August 26, 2011 and accepted October 16, 2011.

Published online October 16, 2011
10.1021/nn203303c

properties to derive five nanodescriptors representing the molecular forces of the nanomaterials interaction with the biological components.[12] The nanodescriptors are intrinsic properties of the nanomaterials that will not change in reversible adsorption processes[12,13] and therefore can be used for quantitative structure −activity relationship (QSAR) model development, nanomedicine delivery, and risk assessment and safety evaluation of nanomaterials.[14,15]

We have mapped the surface adsorption forces over 16 different nanomaterials. The data process for obtaining the nanodescriptors was briefly introduced using multiwalled carbon nanotubes (MWCNT) with diameters of 40 nm and carboxyl (−COOH) surface derivatives as an example. The predictive model development and model validation for a given nanomaterial is described. The five-dimensional nanodescriptor index describing the five types of molecular interactive forces was reduced to two-dimensional *via* principal component analysis, which allows different nanomaterials to be clustered by their surface adsorption properties. The potential applications and predictions as well as considerations and limitations of the BSAI approach are addressed.

RESULTS AND DISCUSSION

In this study, a set of 28 compounds with diverse physicochemical properties were used as probe compounds. The adsorption coefficients (*k*) of the probe compounds on a given nanomaterial (*e.g.*, MWCNT40nm-COOH) were measured using a solid phase microextraction (SPME)-GC/MS method. The log *k* values of the probe compounds and their solute descriptors [*R*, π, α, β, *V*] are provided in the Supporting Information Table S1. The solute descriptors of the probe compounds were obtained from a database as described in the Methods section. The correlation of log *k* with the solute descriptors was established *via* multiple linear regression analysis of the [log k_i, R_i, π_i, α_i, β_i, V_i] matrix,[16,17] where *i* (= 1, 2, 3, ... 28) represents the number of probe compounds

$$\log k = -3.94 + 0.41R + 2.30\pi - 0.51\alpha - 3.59\beta + 6.59V \quad (1)$$

$$n = 28, R^2 = 0.95, F = 91, Q^2_{LOO} = 0.923 \text{ and } Q^2_{LMO25\%} = 0.908$$

Equation 1 is the predictive model for MWCNT40nm-COOH adsorption of chemicals and biomolecules, and the regression coefficients are the nanodescriptors representing five types of molecular interaction forces of the nanomaterial.[12] The relative strength of the five nanodescriptors is depicted in Figure 1. The lipophilicity interaction (*v* = 6.59) is a strong contributor. Hydrogen-bond basicity (*b* = −3.59) is the second significant factor but has a negative value, which reveals that the sorbent surface has a weaker tendency to donate protons (to the probe compounds) than water at the nano-water interface. Hydrogen-bond acidity (*a* = −0.51) has a slight negative value, indicating the proton acceptor strength of the sorbent surface is slightly weaker than water. The third strong factor was the dipolarity/polarizability (*p* = 2.30), which is an attribute of the huge π-electron clouds on the carbon nanotubes.[3,18] The lone-pair electrons (*r* = 0.41) showed a minimum effect, which could be due to the fact that the lone-pair electrons in MWCNT40nm-COOH are shielded inside the π-electron clouds, resulting in little effect on the intermolecular adsorption processes. The BSAI approach not only provides rational interpretations for

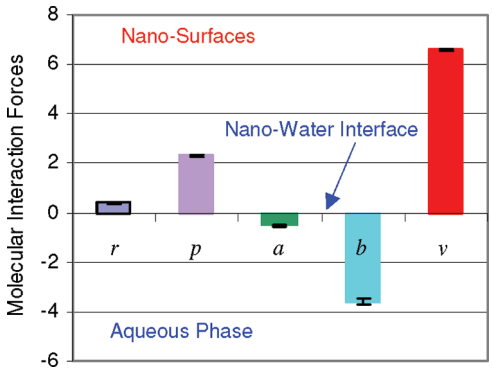

Figure 1. Nanodescriptors [*r*, *p*, *a*, *b*, *v*] measured by the BSAI approach represent the five major molecular interaction forces in the nanoparticle adsorption processes: lone-pair electrons, polarity/polarizability, hydrogen-bond donor, hydrogen-bond acceptor, and London dispersion, respectively. The nanodescriptors of MWCNT40nm-COOH are depicted with standard errors of nine replicate measurements. Positive values indicate that the nanoparticle surfaces have stronger interaction potentials with the chemicals or biomolecules, while negative values indicate that the molecular interactions are stronger in the aqueous phase.

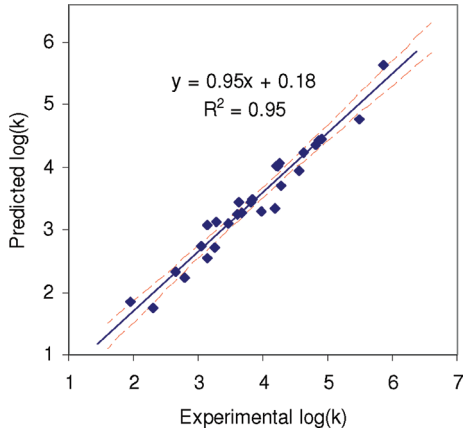

Figure 2. Predicted *versus* measured log *k* values of the probe compounds. The predicted log *k* values were obtained by the nanodescriptors of MWCNT40nm-COOH and the solute descriptors of the probe compounds *via* eq 1. The predicted adsorption coefficients were well-correlated with the experimental measured values with R^2 of 0.95 and $p < 0.0001$. The dashed red lines are the 95% confidence intervals.

the molecular interactions but also provides five quantitative physicochemical parameters characterizing the relative strengths of the molecular interactions of the nanomaterials in the adsorption processes.

The predicted log *k* values by the five nanodescriptors for MWCNT40nm-COOH *versus* the measured log *k* values are shown in Figure 2. A linear correlation was obtained with a correlation coefficient (R^2) of 0.95 and *p* value <0.0001. The dashed red lines are the 95% confidence intervals of the predictive model (eq 1) for MWCNT40nm-COOH. The partial regression plots and regression residual plot (see Supporting Information Figures S1 and S2) showed that the regression model (eq 1) well-described the experimental data.[19,20] The robustness of the model was tested by internal cross-validation using the leave-one-out (LOO) and leave-many-out (LMO25%) techniques[21,22] with validation coefficients Q^2_{LOO} of 0.923 and $Q^2_{LMO25\%}$ of 0.908, respectively (eq 1). Both of the cross-validation coefficients were greater than 0.7, revealing the robustness of the predictive model (see Methods).[21] The external validation of the BSAI approach using 12 different compounds provided an external validation coefficient Q^2_{ext} of 0.78 described in our previous report,[12] suggesting satisfactory predictivity for external validation compounds.[21,23]

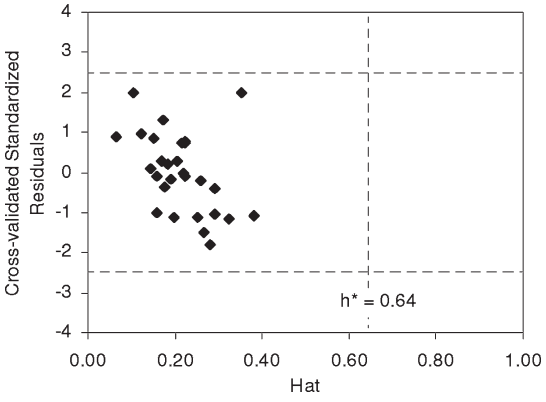

Figure 3. Applicable chemical domain depicted by Williams plot for the model eq 1. If the cross-validated standardized residuals are greater than 2.5 times the standard deviation units (±2.5δ, dashed horizontal lines), the compound will be treated as outliers; if the leverage of a compound greater than the warning leverage (h^* = 0.64, dashed vertical line), the compound is too influential to be included in the model. The log *k* values for all 28 probe compounds are all within the chemical domain, suggesting no outliers and the model predictivity is reliable.[21]

The applicability chemical domain of the model (eq 1) was verified by using Williams plot[21] (Figure 3). If the cross-validated standardized residuals are greater than 2.5 times the standard deviation units (±2.5δ, dashed horizontal lines), the compounds will be treated as outliers; furthermore, if the leverage of a compound is greater than the warning leverage (h^* = 0.64, dashed vertical line), this suggests that the compound is too influential to be included in the model.[21] The log *k* values for all 28 probe compounds were within the chemical domain (Figure 3), suggesting no outliers and the model predictivity was reliable.[21] It is noted that the applicable domain of the model was closely related to the chemical space of the probe compounds. Therefore, the probe compounds should be selected to cover a wide range of physicochemical properties.

TABLE 1. BSAI Nanodescriptors of Nanomaterials

entry	nanomaterial[a]	*n*	R^2	*r*	*p*	*a*	*b*	*v*	PC-1	PC-2
1	s-MWCNT	28	0.92	0.09	2.34	−0.44	−3.06	5.26	1.14	−0.09
2	C_{60} (powder)	28	0.91	0.50	−0.75	−1.23	−2.89	2.85	−0.89	−1.93
3	MWCNT-OH	28	0.90	0.70	2.37	−0.28	−2.45	4.63	0.74	−0.74
4	l-MWCNT	28	0.92	−0.15	2.88	−0.47	−2.79	6.63	1.57	0.26
5	MWCNT 8nm-COOH	28	0.93	−0.10	1.85	0.18	−3.23	6.64	1.39	0.86
6	MWCNT 15nm-COOH	28	0.92	0.64	2.68	−0.17	−3.03	5.81	1.51	−0.54
7	MWCNT 40nm-COOH	28	0.95	0.41	2.30	−0.51	−3.59	6.59	1.82	−0.70
8	carbon hollow sphere	28	0.91	−0.47	3.00	−0.21	−4.07	7.16	2.42	1.00
9	r-graphene oxide	28	0.92	0.68	0.38	−0.79	−1.13	3.05	−1.27	−1.49
10	Ag-silica	22	0.69	−0.99	0.52	0.35	−1.19	0.85	−2.00	2.42
11	Ag-carbon	20	0.74	0.14	0.26	0.21	−1.81	2.02	−1.30	0.52
12	C_{70}TGA	28	0.95	−0.16	−0.59	−1.63	−2.79	1.15	−1.45	−1.39
13	$nC_{60}(OH)_{20}$	28	0.84	−0.45	0.64	0.32	−3.86	2.49	0.02	1.49
14	$nC_{60}(OH)_{32}$	28	0.98	0.08	−0.03	−0.66	−3.34	4.57	0.08	−0.60
15	SiO_2	26	0.78	0.13	−0.33	−0.27	−1.20	0.78	−2.23	−0.07
16	TiO_2	26	0.84	0.10	−0.13	0.57	−1.94	1.39	−1.56	0.99

[a] The characterization and properties of the nanomaterials are detailed in Supporting Information Table S2. The number of probe compounds (*n*) used for the multiple linear regression analysis to obtain five nanodescriptors [*r*, *p*, *a*, *b*, *v*] for each of the nanomaterials with a regression coefficient (R^2). PC-1 and PC-2 are the two components obtained in principal component analysis of the five nanodescriptors for two-dimensional presentation of the molecular interaction forces across the 16 nanomaterials.

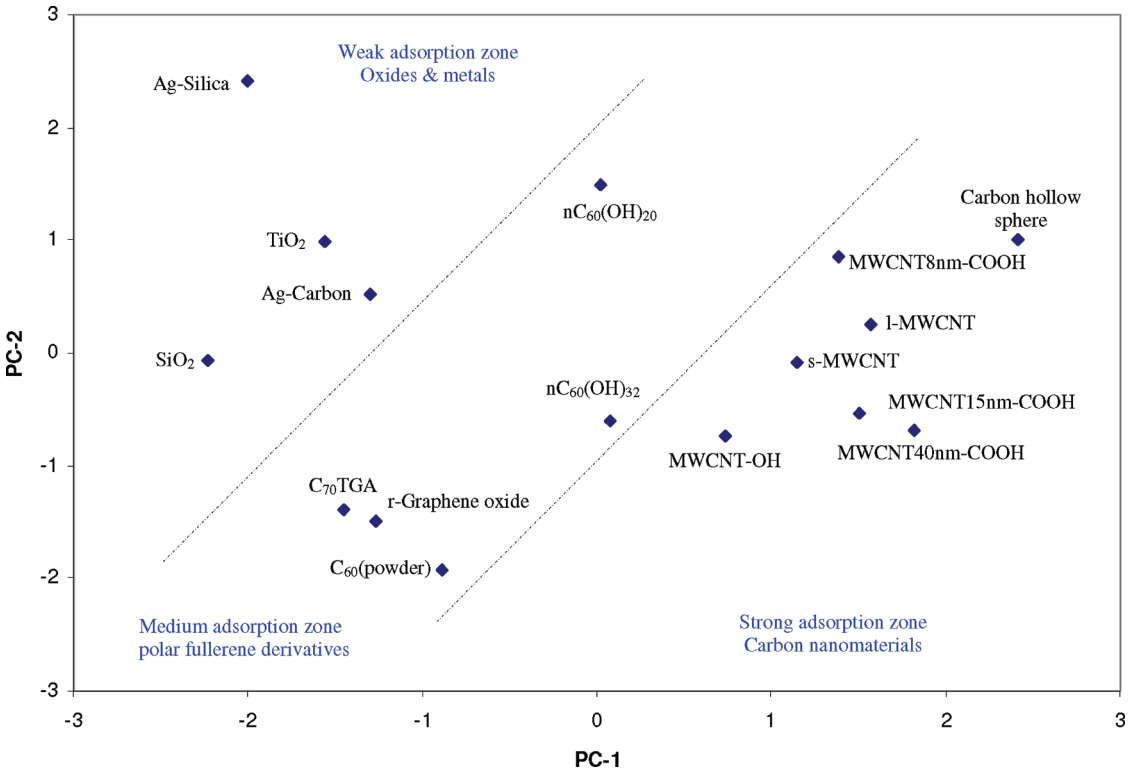

Figure 4. Nanoparticle scattering plot by two principal components. The two components were obtained by principal component analysis of the five nanodescriptors of 16 nanomaterials listed in Table 1. The 16 different nanomaterials were clustered roughly to three zones by their surface adsorption properties.

The 28 probe compounds are widely used chemicals for QSAR model development.[24−26] Due to the great varieties of nanomaterials, different sets of probe compounds may be needed for accurate determination of the log *k* values. The measurement accuracy of the log *k* values of the probe compounds would ultimately determine the quality of the nanodescriptors for the nanomaterial.

We have used the approach illustrated above to measure the nanodescriptors for 16 defined nanomaterials used in a number of our research projects. The properties and characterization of the nanomaterials are given in the Methods section and Supporting Information Table S2. The same experimental protocols and probe compounds used for MWCNT40nm-COOH were used to measure the nanodescriptors for the 16 nanomaterials listed in Table 1. However, for some of the nanomaterials, the adsorption of some of the probe compounds were too weak to be measured accurately; therefore, these compounds were excluded during multiple regression analyses. This lack of adsorption of specific probes is reflective of these nanomaterial surface interactions. The number of compounds (*n*) used in the regression analysis and the R^2 value for each of the nanomaterials are given in Table 1. The nanodescriptors for a given nanomaterial can be used to construct the predictive model for the nanomaterial similar to the predictive model (eq 1) for MWNCT40nm-COOH using data from entry 7, Table 1. A few oxide and metal nanomaterials were also included for diversity, while their nanodescriptor values reflect larger errors as seen in the low regression R^2 values due to the weak adsorption of the probe compounds on these nanomaterials. A different set of probe compounds optimized for these metal oxides would need to be developed for optimal characterization.

The five nanodescriptors defined a five-dimensional matrix of molecular interaction forces for a given nanomaterial. One type of molecular interaction could be a million times stronger than the others; for example, the hydrophobicity interaction for MWCNT40nm-COOH was strong with a *v* value of 6.59, while its hydrogen donor interaction was weak with *a* value of 0.41 (eq 1 and Table 1). On the other hand, one type of molecular interaction could be weak on one nanomaterial but relatively strong for other nanomaterials depending on the nature of the nanomaterials. The BSAI approach uses five nanodescriptors in the model for their clear physicochemical representations and for the cross comparison among different nanomaterials. This is different from pure regression model development where the weaker variables should be removed from the regression model.[27] However, it should be noted that the weak nanodescriptors borne larger errors even though they were not detrimental to the overall predictive model. The quality of the predictive model was reflected by the R^2 value of the regression analysis.

For visual presentation and a clear comparison of diverse nanomaterials, the five-dimensional information can be reduced to two-dimensional *via* principal component analysis of the five nanodescriptors. The principal component analysis was performed to orthogonally transform the five-dimensional data set to two principal components, with the first principal component accounting for as much of the variability in the data as possible and the second component explaining the highest variance possible under the constraint that it be orthogonal to the first component.[28] The two components generated through principal component analysis of the nanodescriptors of the 16 nanomaterials are listed in the last two columns in Table 1. A two-dimensional plot of the two principal components (CP-1 *versus* CP-2) is shown in Figure 4. The 16 nanomaterials can be roughly clustered as strong adsorption nanomaterials including carbon hollow spheres, carbon nanotubes and their derivatives, medium adsorption nanomaterials including C_{60} (powder), polar derivative of fullerenes and graphene oxides, and weak adsorption nanomaterials including oxide and metal nanoparticles. This two-component reduction of the five descriptor index provides a simpler characterization of nanomaterial surface properties, which may be useful for the categorization of biological effects based on surface properties.

The values of nanodescriptors are derived based on the weight of the nanomaterials. Therefore, they can directly correlate with the biological activity in weight-based dose quantities. This overcomes the difficulties in measuring surface area of nanomaterials under biological conditions. In fact, the surface area measured using the conventional BET method[29] could lose its physical meaning in biological conditions due to agglomeration and aggregation of nanomaterials in biological conditions.[30,31] For example, C_{60} (powder) is composed of pristine fullerenes in powder form while it is located in the polar derivative zone. This is because C_{60} (powder) was in the form of large crystals with surface area significantly smaller than molecular C_{60}; therefore, its adsorption energy was significantly reduced. In fact, the BSAI nanodescriptors reflect the real aggregation state of the measurement in the solution, not the conceptual size or particle sizes in purified forms before dose preparation. This has a significant advantage in predicting effects under *in situ* biological conditions.

The direct and simplest application of the BSAI nanodescriptors is to predict the adsorption of small molecules onto the surfaces of nanoparticles. We have demonstrated in our prior report[12] that the measured affinity coefficients (log K_f) of polycyclic aromatic hydrocarbons onto MWCNT[32] were well-correlated with the predicted log *k* values using the BSAI model with a correlation coefficient R^2 of 0.99, and the correlation of the log K_f values of synthetic organic compounds onto single-walled carbon nanotubes[33] with the predicted log *k* values provided R^2 of 0.86. However, there is limited quantitative data of biological activities available for development of such correlations or predictive models, relating surface properties described by the BSAI index to more complex interactions, including aggregation and protein adsorption of nanomaterials in biological systems. We envision the BSAI descriptors to be used as a multivariate index of potential biological interactions, much as the log octanol/water partition coefficient is used for small organics. We present the BSAI data in this report to facilitate development of such models.

Another potential application of the nanodescriptors is to define the toxicity thresholds of nanomaterials. The strong adsorption of proteins onto the nanomaterial surfaces could result in irreversible adsorption. This could lead to the formation of a biocompatible coating making the nanomaterial nontoxic in biological systems. Carbon nanomaterials (carbon nanotubes and hollow spheres) have very hydrophobic surface (*v* term >5, Table 1); irreversible adsorption with proteins is postulated by the BSAI characterization data, which could render such carbon nanomaterials nontoxic in biological systems. This prediction calls for clarification of some toxicity studies of carbon nanomaterials to identify the true cause for observed toxicities reported in the literature; for example, the toxicity from leached metal ions would not attribute to the carbon nanomaterial itself.[34−36] On the other hand, binding of certain proteins, such as complement factors, to the surface of carbon nanomaterials could also lead to adverse immunological effects.[37] The adsorption of proteins could lead to protein changes in higher degrees such as conformation, unfolding, or new epitopes,[6] which could cause new biological consequences. Clearly, then, there is a need for a rational approach to predict such events.

It also worthy to note that hydroxyl and carboxyl derivatization of MWCNTs significantly increased its suspension stability in aqueous media, while their surface adsorption property was not significantly altered. This could be due to the fact that the main polar derivatization sites occurred at the ends of MWCNT while the adsorption property of tube surfaces was not significantly altered. Therefore, carbon nanotubes may be envisioned as drug carriers *via* tube surface adsorption of the drugs.[38] This also explains one of the differences between carbon nanotubes and asbestos, which has hydrophilic surfaces that could not form a strong adsorbed protein layer.[39−42]

It is crucial to define the threshold of how strong the nanoparticle adsorption of proteins could occur reversibly, particularly, when the released proteins are denatured at the adsorption sites. The site-denatured proteins could lose their biological function or acquire unwanted functions.[43−45] Indeed, a recent study has

demonstrated gold-nanoparticle-induced unfolding of fibrinogen resulting in pro-inflammatory effects in an *in vitro* model.[46] The BSAI nanodescriptors representing the adsorption forces could be used to define such adsorption criteria for toxicity assessment and safety evaluation of nanomaterials.

The characterization of nanomaterials as they actually exist in the biological milieu is complicated by complex adsorption of proteins and other biomolecules onto the external surfaces of the nanomaterials.[1,47] In the recently developed nanoparticle−protein corona concept, it was argued that nanoparticles are always coated with proteins and other biomolecules.[6−8] The strongly adsorbed protein on the nanoparticles forms a "hard" corona with a relatively stable protein layer, while the weakly adsorbed the protein forms a "soft" corona that dynamically exchanges with those in the biological milieu.[48] It is the nanoparticle−protein corona that represents the biological identity of the nanomaterial rather than the nanomaterial itself.[1] This concept has been widely accepted in the field of bionanoscience, but it is not clear which factors govern the adsorption affinity or selectivity of proteins in the corona formation process. Also, it is not known which factors govern the exchange of the corona proteins with those in the media. If the adsorption forces of the nanomaterials ultimately govern the affinity and selectivity of proteins, the quantitative BSAI nanodescriptors representing the adsorption forces of nanoparticles can be used to predict the protein affinity and selectivity in a corona formation process. The application of the BSAI nanodescriptors measured using small probe molecules for affinity prediction of proteins is based on the intrinsic nature of free energy related properties. However, the free energy related quantities only describe the thermodynamic contribution of the adsorption driving forces; the adsorption kinetics or mechanisms cannot be described by the nanodescriptors. Particularly, the higher degree changes in proteins such as conformation, unfolding, or new epitopes in the corona formation process are not reflected by the thermodynamic parameters, which should be a subject for the new emerging bionanoscience.[46,49]

Nanomaterials have multiple dimensional physicochemical properties including particle size, shape, surface charge, surface chemistry, core material composition, crystallinity, and structure. The diversity of these properties forms a virtual unlimited number of types of nanomaterials that could be constructed. Each of the nanomaterials could have complicated interactions with proteins and other biomolecules. When faced with such an infinite nanomaterial matrix, a strategic question is how much information is required to describe behavior the nanomaterials in biological systems.[1−3,50] As seen in the two-dimensional principal component reduction of the BSAI index values, clustering of diverse nanomaterials is possible based on surface adsorption properties.

We have postulated that the surface adsorption energy is the primary driving forces behind all of these complicated interactions and dynamic changes of nanomaterials in biological systems. The surface adsorption characteristics of nanomaterials should be one of the basic properties in nanomaterial characterization in addition to the characterization of the physical properties (particle size, size distribution, shape, surface area, *etc.*) and biochemical properties (specific antibody and antigen interactions, specific chemical interactions, oxidative reduction, complexion coordination, *etc.*). Moreover, the surface adsorption forces of nanomaterials govern the absorption, disposition, metabolism, excretion, and pharmacokinetic properties of nanomaterials in nanomedicine applications.[51−53] This is the first success in quantitative characterization of the surface adsorption forces of nanomaterials in biological conditions, which could open a quantitative avenue in predictive nanomedicine development, risk assessment, and safety evaluation of nanomaterials.

METHODS

The nanomaterials were used in our research projects, short MWCNT (s-MWCNT) with a length of 2 μm and long MWCNT (l-MWCNT) with a length of 50 μm, were nonderivatized nanomaterials. Carboxylated MWCNTs with different diameters (<8, 10−20, and 30−50 nm) are labeled as MWCNT8nm-COOH, MWCNT15nm-COOH, and MWCNT40nm-COOH, respectively. MWCNT-OH was a hydroxylated MWCNT with a diameter of 8−15 nm. C_{60} (powder) was pristine fullerene fine powder supplied from the manufacturer. C_{70}-TGA was a fullerene derivative with three tetraglycolic acids (TGA) on each end of the C_{70}-buckyball. $nC_{60}(OH)_{20}$ and $nC_{60}(OH)_{32}$ were in-house (North Carolina State University) prepared nC_{60} nanoparticles with different amounts of hydroxyl groups on the surface fullerenes. Carbon hollow sphere and reduced graphene oxides (r-graphene oxide) were prepared at the University of Cologne. Silica-coated silver (Ag-Silica) and carbon-coated silver (Ag-carbon) nanoparticles were synthesized by NanoComposix. The oxide nanoparticles (TiO_2 and SiO_2) were purchased from SigmaAldrich. The properties and suppliers of the nanomaterials are listed in Supporting Information Table S2.

The adsorption coefficients of the probe compounds were measured using a solid phase microextraction (SPME) and gas chromatography with mass spectrometry (GC/MS) method. A given quantity of nanomaterial (*e.g.*, 2.00 mg of MWCNT40nm-COOH) was weighed into 2 mL vials filled with 200 μL of deionized water. The nanomaterial in water was dispersed in a sonicator bath for 5 min. After sonication, a standard solution (1.00 mL) containing the probe compounds of interest in 12 mM phosphate buffer (pH 7.4) was measured into the vials that were sealed immediately with a Teflon-lined septa cap to reduce evaporation loss of the probe compounds. The adsorption was conducted by shaking the vials containing nanomaterials in the solution of probe compounds on a rotary shaker for 5 h for equilibrium adsorption or different time intervals for kinetic

experiments. The vials were then placed on the sample holder of the autosampler for direct SPME-GC/MS analysis. The SPME technique has high analytical sensitivity; it measures the free concentrations of the probe compounds in the solution without disturbing the adsorption equilibrium, nor the need to separate the nanoparticles from the solution, which is the most difficult step in nanoparticle adsorption of small molecules. The GC/MS method offers a high separation power; multiple chemical compounds can be chromatographically separated and quantitated simultaneously,[54] which is particularly useful for mimicking the competitive adsorption of biomolecules. The robotic automatic sample analysis enables high-throughput generation of the quantitative data.

For quantitative analysis of the 28 probe compounds, polydimethylsiloxane/divinylbenzene (PDMS/DVB) membrane-coated fibers showed an optimal performance. Only parts per billion levels of the probe compounds (individual concentrations) were required because of the high analytical sensitivity of the SPME-GC/MS method.[12] The equilibrium concentration (C_e) of the probe compounds in the solution were determined in the quantitative analysis. The adsorption amounts (n^e) of the probe compounds by the nanoparticles were obtained by subtracting the quantities remaining in the solution from the dosed amounts in the standard solution ($n^e = V_0C_0 - V_eC_e$), where C_0 is the standard concentration of a probe compound and V_0 is the volume. The surface concentration (C_{ad}) of the probe compound adsorbed on the nanoparticle surfaces is calculated from the adsorption amount (n^e) and the mass (m) of the nanomaterial in the testing solution ($C_{ad} = n^e/m$). The adsorption constant (k) of a given probe compound is the ratio of surface concentration (C_{ad}) *versus* the equilibrium concentration (C_e) in the solution

$$k = \frac{C_{ad}}{C_e} = \frac{V_0C_0 - V_eC_e}{mC_e} \quad (2)$$

The nanodescriptors for a given nanomaterial were obtained by multiple linear regression analysis of the [log k, R, π, α, β, V] matrix *via* eq 1. The log k values were measured *via* the adsorption experiments, and the solute descriptors were provided by the Absolv program in ADME Suite software (Advanced Chemistry Development Inc., Toronto, Canada). An example of the [log k, R, π, α, β, V] matrix for MWCNT40nm-COOH is given in Supporting Information Table S1. The regression analysis was performed by using the Analyst program in SAS software (SAS Institute Inc., Cary, NC).

The robustness of the model (eq 1) was studied by internal cross-validation using the leave-one-out (LOO) and leave-many (25% of the data)-out (LMO25%) techniques. The validation coefficients (Q^2_{LOO}) < 0.7 indicate models with low robustness and low internal predictive ability; $Q^2_{LMO25\%}$ is a stronger cross-validation coefficient than Q^2_{LOO}.[21] The applicability domain of the predictive models was verified by the leverage approach using a Williams plot, the leverages of the chemicals (diagonal elements of the Hat matrix) *versus* the Euclidean distances of the compounds to the models measured by the jackknifed (standardized and cross-validated) residuals.[21,23] If the jackknifed residual of a compound is greater than 2.5 times the standard deviation units ($\pm 2.5\sigma$), the compound will be treated as outliers. If the leverage of the compound is greater than the warning leverage ($h > h^*$), it suggests that the compound is very influential on the model. The warning leverage is defined as $h^* = 3(N + 1)/n$, where N is the number of independent variables in the predictive model ($N = 5$ in eq 1) and n is the number of probe compounds ($n = 28$ in this study).

Acknowledgment. This research was supported by the United States Environmental Protection Agency (USEPA) STAR Grant No. R833328, the United States Air Force Office of Scientific Research (USAOSR) Grant No. FA9550-08-1-0182, and the National Institutes of Health (NIH) R01 ES016138 and FP7-NANOMMUNE (Grant Agreement No. 214281). The authors thank Jim Brooks for help in QSAR validation techniques, and Jim Yeatts for analytical chemistry support.

Supporting Information Available: Methods and supplementary figures. This material is available free of charge *via* the Internet at http://pubs.acs.org.

REFERENCES AND NOTES

1. Nel, A. E.; Mädler, L.; Velegol, D.; Xia, T.; Hoek, E. M.; Somasundaran, P.; Klaessig, F.; Castranova, V.; Thompson, M. Understanding Biophysicochemical Interactions at the Nano-Bio Interface. *Nat. Mater.* **2009**, *8*, 543–557.
2. Hall, J. B.; Dobrovolskaia, M. A.; Patri, A. K.; McNeil, S. E. Characterization of Nanoparticles for Therapeutics. *Nanomedicine* **2007**, *2*, 789–803.
3. Lynch, I.; Cedervall, T.; Lundqvist, M.; Cabaleiro-Lago, C.; Linse, S.; Dawson, K. A. The Nanoparticle—Protein Complex as a Biological Entity; A Complex Fluids and Surface Science Challenge for the 21st Century. *Adv. Colloid Interface Sci.* **2007**, *134—135*, 167–174.
4. Montes-Burgos, I.; Walczyk, D.; Hole, P.; Smith, J.; Lynch, I.; Dawson, K. A. Characterisation of Nanoparticle Size and State Prior to Nanotoxicological Studies. *J. Nanopart. Res.* **2010**, *12*, 47–53.
5. Kendall, M.; Ding, P.; Kendall, K. Particle and Nanoparticle Interactions with Fibrinogen: The Importance of Aggregation in Nanotoxicology. *Nanotoxicology* **2011**, *5*, 55–65.
6. Lynch, I.; Dawson, K. A.; Linse, S. Detecting Cryptic Epitopes Created by Nanoparticles. *Sci. STKE* **2006**, *327*, 14.
7. Cedervall, T.; Lynch, I.; Lindman, S.; Berggård, T.; Thulin, E.; Nilsson, H.; Dawson, K. A.; Linse, S. Understanding the Nanoparticle—Protein Corona Using Methods To Quantify Exchange Rates and Affinities of Proteins for Nanoparticles. *Proc. Natl. Acad. Sci. U.S.A.* **2007**, *104*, 2050–2055.
8. Lynch, I.; Dawson, K. A. Protein—Nanoparticle Interactions. *Nano Today* **2008**, *3*, 40–47.
9. Verma, A.; Stellacci, F. Effect of Surface Properties on Nanoparticle—Cell Interactions. *Small* **2010**, *6*, 12–21.
10. Mailänder, V.; Landfester, K. Interaction of Nanoparticles with Cells. *Biomacromolecules* **2009**, *10*, 2379–400.
11. Patil, S.; Sandberg, A.; Heckert, E.; Self, W.; Seal, S. Protein Adsorption and Cellular Uptake of Cerium Oxide Nanoparticles as a Function of Zeta Potential. *Biomaterials* **2007**, *28*, 4600–4607.
12. Xia, X. R.; Monteiro-Riviere, N. A.; Riviere, J. E. An Index for Characterization of Nanomaterials in Biological Systems. *Nat. Nanotechnol.* **2010**, *5*, 671–675.
13. Kamal Al-Malah, K. Modeling of Protein Adsorption Equilibrium at Hydrophobic Solid—Water Interfaces. In *Adsorption: Theory, Modeling, and Analysis*; József Tóth, J., Ed.; Marcel Dekker: New York, 2002; pp 803—847.
14. Puzyn, T.; Leszczynska, D.; Leszczynski, J. Toward the Development of "Nano-QSARs": Advances and Challenges. *Small* **2009**, *5*, 2494–2509.
15. Aillon, K. L.; Xie, Y.; El-Gendy, N.; Berkland, C. J.; Forrest, M. L. Effects of Nanomaterial Physicochemical Properties on *In Vivo* Toxicity. *Adv. Drug Delivery Rev.* **2009**, *61*, 457–466.
16. Abraham, M. H. Scales of Solute Hydrogen-Bonding: Their Construction and Application to Physicochemical and Biochemical Processes. *Chem. Soc. Rev.* **1993**, *22*, 73–83.
17. Karelson, M., Ed. *Molecular Descriptors in QSAR/QSPR*: John Wiley & Sons, Inc.: New York, 2000.
18. Arkin, M. R.; Stemp, E. D.; Holmlin, R. E.; Barton, J. K.; Hörmann, A.; Olson, E. J.; Barbara, P. F. Rates of DNA-Mediated Electron Transfer between Metallointercalators. *Science* **1996**, *273*, 475–480.
19. Xia, X. R.; Baynes, R. E.; Monteiro-Riviere, N. A.; Riviere, J. E. A System Coefficient Approach for Quantitative Assessment of the Solvent Effects on Membrane Absorption from Chemical Mixtures. *SAR QSAR Environ. Res.* **2007**, *18*, 579–593.
20. Peck, R., Olsen, C., Devore, J. L., Eds. *Introduction to Statistics and Data Analysis*; Cengage Learning, Brooks/Cole: Belmont, CA, 2011.
21. Gramatica, P. Principles of QSAR Models Validation: Internal and External. *QSAR Comb. Sci.* **2007**, *26*, 694–701.
22. Dearden, J. C.; Cronin, M. T. D.; Kaiser, K. L. E. How Not To Develop a Quantitative Structure—Activity or Structure—Property Relationship (QSAR/QSPR). *SAR QSAR Environ. Res.* **2009**, *20*, 241–266.
23. Gramatica, P.; Giani, E.; Papa, E. Statistical External Validation and Consensus Modeling: A QSPR Case Study for Koc Prediction. *J. Mol. Graphics Modell.* **2007**, *25*, 755–766.

24. Abraham, M. H.; Chadha, H. S.; Martins, F.; Mitchell, R. C.; Bradbury, M. W.; Gratton, J. A. Hydrogen Bonding Part 46. A Review of the Correlation and Prediction of Transport Properties by an LFER Method: Physicochemical Properties, Brain Penetration and Skin Permeability. *Pestic. Sci.* **1999**, *55*, 78–88.
25. Poole, C. F.; Poole, S. K.; Abraham, M. H. Recommendations for the Determination of Selectivity in Micellar Electrokinetic Chromatography. *J. Chromatogr. A* **1998**, *798*, 207–222.
26. Xia, X. R.; Baynes, R. E.; Monteiro-Riviere, N. A.; Riviere, J. E. An Experimental Based Approach for Predicting Skin Permeability of Chemicals and Drugs Using a Membrane-Coated Fiber Array. *Toxicol. Appl. Pharmacol.* **2007**, *221*, 320–328.
27. Rawlings, J. O., Pantula, S. G., Dickey, D. A., Eds. *Applied Regression Analysis: A Research Tool*; Springer: New York, 1998.
28. Jolliffe, I. T., Ed. *Principal Component Analysis*; Springer: New York, 2004.
29. Kaufhold, S.; Dohrmann, R.; Klinkenberg, M.; Siegesmund, S.; Ufer, K. N(2)-BET Specific Surface Area of Bentonites. *J. Colloid Interface Sci.* **2010**, *349*, 275–282.
30. Gilbert, B.; Ono, R. K.; Ching, K. A.; Kim, C. S. The Effects of Nanoparticle Aggregation Processes on Aggregate Structure and Metal Uptake. *J. Colloid Interface Sci.* **2009**, *339*, 285–295.
31. Pettibone, J. M.; Cwiertny, D. M.; Scherer, M.; Grassian, V. H. Adsorption of Organic Acids on TiO_2 Nanoparticles: Effects of pH, Nanoparticle Size, and Nanoparticle Aggregation. *Langmuir* **2008**, *24*, 6659–6667.
32. Yang, K.; Wang, X.; Zhu, L.; Xing, B. Competitive Sorption of Pyrene, Phenanthrene, and Naphthalene on Multiwalled Carbon Nanotubes. *Environ. Sci. Technol.* **2006**, *40*, 5804–5810.
33. Zhang, S.; Shado, T.; Bekaroglu, S. S.; Karanfil, T. The Impacts of Aggregation and Surface Chemistry of Carbon Nanotubes on the Adsorption of Synthetic Organic Compounds. *Environ. Sci. Technol.* **2009**, *43*, 5719–5725.
34. Lam, C. W.; James, J. T.; McCluskey, R.; Arepalli, S.; Hunter, R. L. A Review of Carbon Nanotube Toxicity and Assessment of Potential Occupational and Environmental Health Risks. *Crit. Rev. Toxicol.* **2006**, *36*, 189–217.
35. Pulskamp, K.; Diabaté, S.; Krug, H. F. Carbon Nanotubes Show No Sign of Acute Toxicity but Induce Intracellular Reactive Oxygen Species in Dependence on Contaminants. *Toxicol. Lett.* **2007**, *168*, 58–74.
36. Rana, S.; Yeh, Y. C.; Rotello, V. M. Engineering the Nanoparticle−Protein Interface: Applications and Possibilities. *Curr. Opin. Chem. Biol.* **2010**, *14*, 828–834.
37. Rybak-Smith, M. J.; Sim, R. B. Complement Activation by Carbon Nanotubes. *Adv. Drug Delivery Rev.* **2011**, *63*, 1031–1041.
38. Kostarelos, K.; Bianco, A.; Prato, M. Promises, Facts and Challenges for Carbon Nanotubes in Imaging and Therapeutics. *Nat. Nanotechnol.* **2009**, *4*, 627–633.
39. Shvedova, A. A.; Kisin, E. R.; Porter, D.; Schulte, P.; Kagan, V. E.; Fadeel, B.; Castranova, V. Mechanisms of Pulmonary Toxicity and Medical Applications of Carbon Nanotubes: Two Faces of Janus? *Pharmacol. Ther.* **2009**, *121*, 192–204.
40. Bianco, A.; Kostarelos, K.; Prato, M. Applications of Carbon Nanotubes in Drug Delivery. *Curr. Opin. Chem. Biol.* **2005**, *9*, 674–679.
41. Beg, S.; Rizwan, M.; Sheikh, A. M.; Hasnain, M. S.; Anwer, K.; Kohli, K. Advancement in Carbon Nanotubes: Basics, Biomedical Applications and Toxicity. *J. Pharm. Pharmacol.* **2011**, *63*, 141–163.
42. Zhang, Y.; Bai, Y.; Yan, B. Functionalized Carbon Nanotubes for Potential Medicinal Applications. *Drug Discovery Today* **2010**, *15*, 428–435.
43. Fernández, A.; Ramsden, J. J. On Adsorption-Induced Denaturation of Folded Proteins. *J. Biol. Phys. Chem.* **2001**, *1*, 81–84.
44. Rodriguez, C. E.; Fukuto, J. M.; Taguchi, K.; Froines, J.; Cho, A. K. The Interactions of 9,10-Phenanthrenequinone with Glyceraldehydes-3-phosphate Dehydrogenase (GAPDH), A Potential Site for Toxic Actions. *Chem. Biol. Interact.* **2005**, *155*, 97–110.
45. Brevig, T.; Holst, B.; Ademovic, Z.; Rozlosnik, N.; Røhrmann, J. H.; Larsen, N. B.; Hansen, O. C.; Kingshott, P. The Recognition of Adsorbed and Denatured Proteins of Different Topographies by β2 Integrins and Effects on Leukocyte Adhesion and Activation. *Biomaterials* **2005**, *26*, 3039–3053.
46. Deng, Z. J.; Liang, M.; Monteiro, M.; Toth, I.; Minchin, R. F. Nanoparticle-Induced Unfolding of Fibrinogen Promotes Mac-1 Receptor Activation and Inflammation. *Nat. Nanotechnol.* **2011**, *6*, 39–44.
47. Kunzmann, A.; Andersson, B.; Thurnherr, T.; Krug, H.; Scheynius, A.; Fadeel, B. Toxicology of Engineered Nanomaterials: Focus on Biocompatibility, Biodistribution and Biodegradation. *Biochim. Biophys. Acta* **2011**, *1810*, 361–373.
48. Monopoli, M. P.; Walczyk, D.; Campbell, A.; Elia, G.; Lynch, I.; Bombelli, F. B.; Dawson, K. A. Physical-Chemical Aspects of Protein Corona: Relevance to *In Vitro* and *In Vivo* Biological Impacts of Nanoparticles. *J. Am. Chem. Soc.* **2011**, *133*, 2525–2534.
49. Monopoli, M. P.; Bombelli, F. B.; Dawson, K. A. Nanobiotechnology: Nanoparticle Coronas Take Shape. *Nat. Nanotechnol.* **2011**, *6*, 11–12.
50. Maynard, A. D.; Warheit, D. B.; Philbert, M. A. The New Toxicology of Sophisticated Materials: Nanotoxicology and Beyond. *Toxicol. Sci.* **2011**, *120*), S109–S129.
51. Fubini, B.; Ghiazza, M.; Fenoglio, I. Physico-chemical Features of Engineered Nanoparticles Relevant to Their Toxicity. *Nanotoxicology* **2010**, *4*, 347–363.
52. Zolnik, B. S.; Sadrieh, N. Regulatory Perspective on the Importance of ADME Assessment of Nanoscale Material Containing Drugs. *Adv. Drug Delivery Rev.* **2009**, *61*, 422–427.
53. Riviere, J. E. Pharmacokinetics of Nanomaterials: An Overview of Carbon Nanotubes, Fullerenes and Quantum Dots. *WIREs Nanomed. Nanobiotechnol.* **2009**, *1*, 26–34.
54. Xia, X. R.; Baynes, R. E.; Monteiro-Riviere, N. A.; Leidy, R. B.; Shea, D.; Riviere, J. E. A Novel *In-Vitro* Technique for Studying Percutaneous Permeation with a Membrane-Coated Fiber and Gas Chromatography/Mass Spectrometry Part I. Performances of the Technique and Determination of the Permeation Rates and Partition Coefficients of Chemical Mixtures. *Pharm. Res.* **2003**, *20*, 272–279.